Journal of Thermal Analysis and Calorimetry
https://doi.org/10.1007/s10973-026-15620-2

# Modeling the combustion emissions of sustainable aviation fuel blends

**Doğa Kılıç[1,3] · Melih Yıldız[2,3] · Jonas Matijošius[4] · Utku Kale[5,6]**

Received: 29 October 2025 / Accepted: 2 May 2026
© The Author(s) 2026

**Abstract**
Assessing the thermodynamic and environmental performance of alternative fuel blends is crucial for energy management and climate change mitigation within the aviation industry. In this study, a data-driven impact assessment utilizing surrogate models was employed to evaluate the steady-state performance and emission characteristics of a turboprop gas turbine engine. Three synthetic paraffinic kerosene (HEFA, ATJ-SPK, and FT-SPK) blended with conventional Jet-A up to a 50% volumetric ratio were thoroughly investigated. Operating under a constant fuel mass flow rate boundary condition, the enhanced gravimetric energy density of the sustainable aviation fuels (SAFs) yielded a direct mechanical power augmentation, resulting in up to a 1.0% reduction in Specific Fuel Consumption (SFC). The most critical contribution of this research is the isolation and quantification of the "double-benefit" phenomenon through a power-normalized specific emission framework. By integrating the chemical reduction in carbon oxidation with thermodynamic efficiency gains, the results demonstrated that actual operational emissions are significantly lower than mass-balance predictions. At the 50% blend limit, soot formation plummeted by exactly 40%. Furthermore, power-normalized specific emissions demonstrated net operational reductions of 3.1% for $CO_2$ and 3.06% for thermal $NO_x$, which was effectively evaluated via a specialized quadratic surrogate model. Ultimately, this data-driven methodology emerges as a highly predictive and reliable tool for characterizing advanced fuel-engine integrations, facilitating data-driven decision-making to accelerate aviation's transition to clean energy.

**Keywords** Sustainable aviation fuels · Impact analyses · Emissions · Gas turbine engine

## Introduction

In order to lessen the carbon footprint of the aviation industry, sustainable aviation fuels, or SAF, are becoming a more environmentally friendly option than traditional jet fuels [1]. Without changing the structure of the current power plant, drop-in SAF fuels can be used in place of or blended with fossil jet fuel [2]. These fuels, which can be made synthetically or from biomass, lower greenhouse gas emissions by 41% to 89% over the course of their life cycles. They have been demonstrated to cut $SO_2$ emissions by 92% and particulate matter emissions by 70–95% because of their low

✉ Doğa Kılıç
dogak@erciyes.edu.tr

Melih Yıldız
melihy@erciyes.edu.tr

Jonas Matijošius
jonas.matijosius@vilniustech.lt

Utku Kale
kale.utku@kjk.bme.hu

[1] Graduate School of Natural and Applied Sciences, Erciyes University, 38039 Kayseri, Türkiye

[2] Department of Aeronautical Engineering, Faculty of Aeronautics and Astronautics, Erciyes University, 38030 Kayseri, Türkiye

[3] ERHAM-Aviation Application and Research Center, Erciyes University, 38039 Kayseri, Türkiye

[4] Mechanical Science Institute, Vilnius Gediminas Technical University, Plytinės G. 25, 10105 Vilnius, Lithuania

[5] Department of Aeronautics, and Naval Architecture, Faculty of Transportation Engineering and Vehicle Engineering, Budapest University of Technology and Economics, Műegyetem Rkp. 3, 1111 Budapest, Hungary

[6] Vilnius Gediminas Technical University, Plytinės G. 25, 10105 Vilnius, Lithuania

Published online: 24 June 2026

sulfur and aromatic compound content [3]. This rate can surpass 70% with the appropriate selection of raw materials and production methods based on renewable energy [4].

According to the ASTM D7566 standard, SAF includes seven fuels that have been authorized for use in aircraft [5]. By means of multi-level testing, certification under this standard certifies that the fuels, up to a specific blend level, meet the chemical and performance characteristics of conventional petroleum jet fuel [6]. SAF can be approved as DEF STAN 91–91 and ASTM D1655 turbine fuel after being certified by ASTM D7566—17 [7]. Table 1 presents the certified alternative jet fuel pathways, detailing their respective blending limits, feedstocks, and current TRL status for commercial aviation.

## Future perspective

In the short and medium term, sustainable aviation fuels (SAFs) are thought to be the most practical way to lower carbon emissions in the aviation sector [5]. However, the biggest obstacles to the widespread use of these fuels are their high production costs and limited production capacity in comparison to conventional fossil fuels [2, 10]. The supply of raw materials, technological scalability, and the carbon intensity of the energy sources used in production processes are the primary factors driving up production costs [4]. However, it was emphasized that the infrastructure and logistics costs of alternative fuels such as hydrogen also pose a serious barrier to widespread use [11].

Adequate policy frameworks and intensive research and investment to lower SAF production costs are necessary to ensure economic sustainability [10]. Governments must create systems that lower the risks associated with SAF production and make funding more accessible, according to IATA. In this context, the Renewable Energy Directive II of the European Union has implemented a more favorable incentive scheme for aviation as opposed to road transportation [12].

Because electric and hydrogen-powered aircraft technologies are not yet operationally mature, SAFs are positioned as a bridge fuel in the aviation industry's decarbonization process. SAFs stand out as a sustainable transformation tool for the sector to meet its climate goals because of their high degree of compatibility with current engine technologies and infrastructure [5, 8]. However, while SAFs offer a short- to mid-term solution, achieving full decarbonization in the long term will require a shift toward more radical alternatives such as hydrogen and electric propulsion. In this context, for such alternative fuels to be effectively integrated into aviation, current aircraft designs must be optimized in terms of energy integration, aerodynamics, and structural performance [13]. Furthermore, as the aviation industry transitions toward radical alternatives such as hydrogen and electric propulsion, adopting a systems thinking approach becomes imperative for managing the inherent design complexities and ensuring effective energy integration across the aircraft's lifecycle [14].

## Methodology

In this research, the gas turbine engine's individual components—including the compressor, combustion chamber, power turbine, high-pressure turbine, and exhaust—are modeled modularly using a 1D Thermodynamic Engine Model. This modular approach enables flexible, scalable, and rapid assembly of various engine configurations within a virtual environment. Consequently, adjustments at the component level facilitate straightforward analysis and validation of the engine's overall performance. The model accurately simulates the physical engine's operational characteristics and supports real-time simulation based on environmental

**Table 1** Sustainable aviation fuels production pathways [8, 9]

| SAF | Feedstocks | Certification | Blend Limit/%v/v | TRL |
|---|---|---|---|---|
| Fischer–Tropsch synthesized iso-paraffinic kerosene (FT-SPK) | Wastes (MSW, etc.), coal, gas, sawdust | ASTM D7566 Annex1 | 50% | 7—8 |
| Hydroprocessed fatty acid esters and fatty acids (HEFA) | Vegetable oils: palm, camelina, jatropha, used cooking oil | ASTM D7566 Annex2 | 50% | 9 |
| Synthesized iso-paraffins (SIP) | Sugarcane, sugar beet | ASTM D7566 Annex3 | 10% | 7—8 |
| Fischer–Tropsch containing aromatics (FT-SKA) | Wastes (MSW, etc.), coal, gas, sawdust | ASTM D7566 Annex4 | 50% | 7—8 |
| Alcohol to jet (ATJ) | Sugarcane, sugar beet, sawdust, lignocellulosic residues (straw) | ASTM D7566 Annex5 | 50% | 5—8 |
| Catalytic hydrothermolysis jet fuel (CHJ) | Waste oils or energy oils | ASTM D7566 Annex6 | 50% | 5—8 |
| Hydroprocessed hydrocarbons synthesized iso-paraffinic kerosene (HH-SPK or HC-HEFA) | Algal oil | ASTM D7566 Annex7 | 10% | 6 |

factors such as altitude and Mach number. This capability allows for anticipating engine responses under different flight conditions, thereby enabling the evaluation of critical performance and safety decisions in a virtual setting.

## Digital engine modeling and system architecture

To accurately evaluate the system-level impacts of SAF substitution, a high-fidelity, 1D thermodynamic engine model was developed within a physics-based simulation framework. Rather than relying on generic, static performance maps, the architecture explicitly interconnects the thermodynamic cycle, multi-species air–fuel mass flow, and transient mechanical power transfers. This modular approach ensures that localized fluid-thermal variations—driven by the distinct physical properties of the SPK fuels—dynamically propagate through the entire engine cycle.

The predictive model represents a PT6-class turboprop architecture, fundamentally compartmentalized into two main modules: the Gas Generator and the Propeller Dynamics Module. This topology (shown in Fig. 1) allows each subcomponent to be dynamically integrated while mathematically anchored to manufacturer specifications and validated operational boundaries:

- **Compressor:** Evaluates the air mass flow rate, pressure ratio, and isentropic efficiency as dynamic functions of the gas generator shaft speed and variable inlet conditions.
- **Combustion chamber:** Calculates total heat release and exit temperature by actively processing the blend-resolved Lower Heating Value (LHV) and chemical stoichiometry of the SAF blends. This is strictly coupled with the chamber's physical volume, dynamic pressure drop, and instantaneous combustion efficiency.
- **High-pressure and power turbines:** Resolves the mechanical power extracted and transferred to the respective shafts, accounting for isentropic expansion efficiencies based on the transient fluid states at the inlet and outlet.
- **Exhaust:** Determines dynamic pressure recovery and kinetic energy dissipation as the gas flow exits the engine nozzle.
- **Propeller:** Translates mechanical shaft power into aerodynamic performance utilizing manufacturer-derived data, expressing the power coefficient ($C_p$) and thrust coefficient ($C_t$), as functions of the advance ratio (J) and blade pitch angle (β).

By linking these independently modeled subcomponents within the physics-based simulation framework, the Gas Generator Model simulates the complete thermodynamic

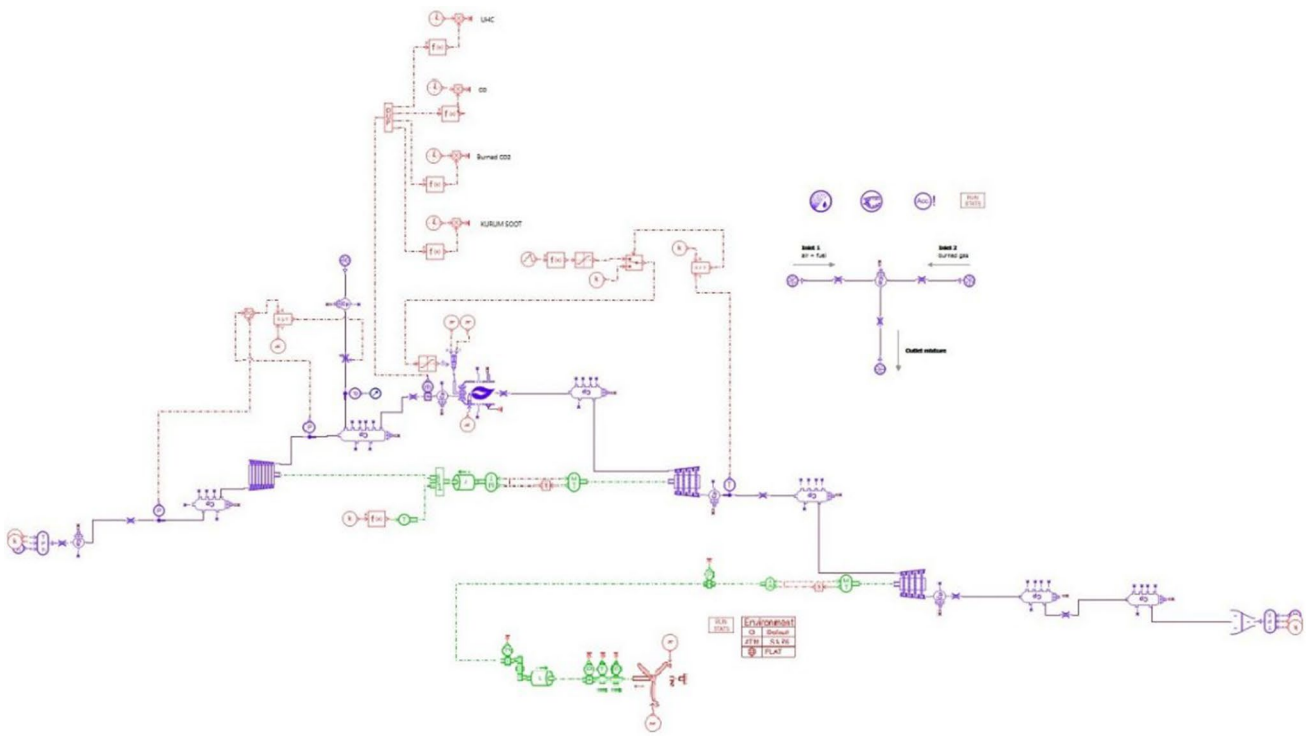

**Fig. 1** Component-level architecture of the baseline 1D thermodynamic turboprop engine model

cycle—from air intake to turbine exhaust. This integrated 1D system architecture continuously calculates critical operational outputs, including torque, fuel flow rate, inter-turbine temperature (ITT), and shaft horsepower (SHP). These outputs are automatically adjusted in response to changing environmental factors.

To maximize engine performance while maintaining a strictly stable and safe operating regime, an advanced engine control algorithm developed at the ERHAM (Erciyes University Aviation Studies Application and Research Center) laboratory was integrated into the simulation framework. This algorithm incorporates a rigorous temperature control mechanism designed to prevent turbine blade overheating. As depicted in Fig. 2, the controller, functioning at elevated shaft speeds, enforces a material limit of 2565°R (approximately 1273 K), representing the absolute target turbine inlet temperature (TIT) that must not be exceeded. Furthermore, the algorithm dynamically regulates the fuel mass flow to prevent lean blow-off during rapid deceleration and strictly limits the operating envelope to ensure the engine does not cross the compressor surge line during acceleration. By precisely calculating the ultimate fuel delivery under these transient constraints, the ERHAM control algorithm averts thermal overloading and aerodynamic instability, thereby guaranteeing safe and efficient operational performance.

## Model calibration and baseline validation

The predictive fidelity of the developed 1D thermodynamic engine model was evaluated through a rigorous calibration procedure against a standard Pratt & Whitney PT6 turboprop baseline. Due to its widespread integration and well-documented operational metrics [15], the PT6 architecture serves as an ideal benchmark. To isolate the engine's mechanical and aerodynamic validity before introducing the complexities of sustainable aviation fuels (SAFs), all initial calibration procedures were strictly conducted using conventional Jet-A.

To establish a reliable comparative baseline, the engine's geometric and operational boundaries were mapped using the industry-standard GasTurb simulation suite. This provided a high-fidelity, literature-validated dataset of steady-state performance outputs. The custom 1D simulation model was then systematically calibrated against these GasTurb-derived reference data, establishing a scientifically transparent and reproducible basis for the subsequent SAF integration.

The thermodynamic and aerodynamic validation of the simulation framework focused on comparing key performance metrics across a comprehensive operational envelope. Specifically, the baseline validation was executed at sea level—encompassing both standard-day (288.15 K) and

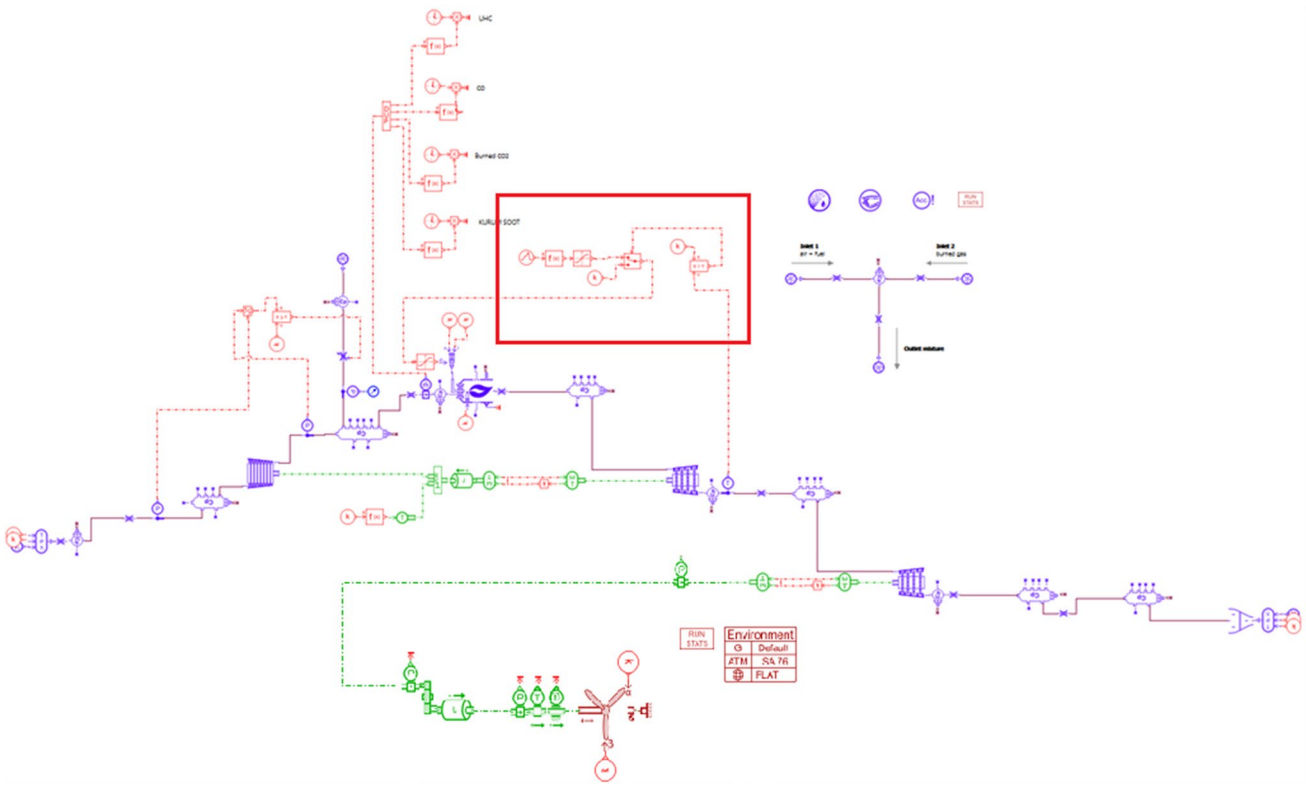


**Fig. 2** Control mechanism for Exhaust Gas Temperature (EGT)

**Table 2** Numerical model validation in a range of flight scenarios and overall error rates

| FLIGHT CONDITIONS | Sea level, 288,15 K | Sea level, 303,15 K | 5000 ft, 288,15 K | 10,000 ft, 261,15 K | AVERAGE ERROR/% |
|---|---|---|---|---|---|
| *Parameters* | *Ref.* \| *1D Model* | *Ref.* \| *1D Model* | *Ref.* \| *1D Model* | *Ref.* \| *1D Model* | |
| GROSS THRUST/*lb* | 256,2 \| 246,2 | 234,8 \| 227 | 266,13 \| 254,46 | 246,27 \| 249,33 | 3,772 |
| OUTPUT TORQUE/*ft—lb* | 5494,9 \| 5299,4 | 3556,5 \| 3718,5 | 4027,58 \| 3832,48 | 3730,67 \| 3928,59 | 4,965 |
| GAS GEN SPEED/*rpm* | 37,098,4 \| 36,951,3 | 38,004 \| 38,134 | 38,036,4 \| 37,545,4 | 36,844 \| 37,119,4 | 2,331 |
| EGT/*K* | 874,92 \| 865,59 | 932 \| 929 | 923,44 \| 922,98 | 872,98 \| 872,03 | 0,607 |
| P1 $_{\text{COMP.INLET}}$/*psi* | 14,678 \| 14,6784 | 14,34 \| 13,42 | 11,96 \| 12,05 | 13,83 \| 14,156 | 2,814 |
| P3 $_{\text{COMP. DELIVERY}}$/*psi* | 147,47 \| 144,477 | 139,5 \| 137,09 | 122,9 \| 133,3 | 136,27 \| 142,56 | 3,609 |
| P7 $_{\text{EXHAUST}}$/*psi* | 14,6959 \| 14,6959 | 16,172 \| 14,6959 | 13,594 \| 12,228 | 15,63 \| 14,173 | 8,475 |

hot-day (303.15 K) conditions to assess thermal sensitivity—as well as at elevated altitudes of 5,000 ft and 10,000 ft. As detailed in the comparative analysis (Table 2), critical operational parameters including gross thrust, output torque, and gas generator speed were systematically evaluated alongside internal thermodynamic stations (compressor inlet P1, compressor delivery P3, exhaust nozzle P7) and Exhaust Gas Temperature (EGT). The custom 1D model demonstrated robust agreement with the reference PT6 data across this entire spectrum, proving its capability to accurately track altitude-induced and thermal performance shifts prior to SAF integration.

Quantitative analysis of the baseline validation revealed exceptional predictive accuracy. The average relative deviations between the 1D model and the GasTurb reference data were strictly constrained to 3.77% for gross thrust, 4.96% for output torque, and a remarkable 0.61% for Exhaust Gas Temperature (EGT). Furthermore, the thermodynamic tracking of internal pressure stations proved highly stable, with maximum deviations constrained below 8.5%. These convergence metrics fall well within the stringent tolerance margins established in contemporary literature for high-fidelity 1D thermodynamic engine models [16, 17]. Ultimately, this comprehensive multi-point calibration ensures that the simulation framework correctly replicates the core thermo-mechanical behavior of the PT6 architecture, establishing a fully validated foundation prior to the introduction of sustainable aviation fuel (SAF) blends.

## Fuel characterization and blend-resolved inputs

In the simulation phase of the study, three sustainable aviation fuels (SAFs) were selected as alternatives to conventional petroleum-based Jet-A fuel: Gevo's Alcohol-to-Jet synthetic paraffinic kerosene (ATJ-SPK), derived from microorganism-based isobutanol; Honeywell UOP's Hydrotreated Esters and Fatty Acids (HEFA-SPK), produced from camelina oil; and Fischer–Tropsch (FT-SPK). The fundamental baseline properties and production pathways of these primary fuels are explicitly detailed in Table 3.

These SAFs were mixed with Jet-A in varying proportions to produce a total of fifteen distinct blends, all strictly adhering to the maximum blending limits specified by the ASTM D7566 standard. To achieve high modeling precision and accurately capture the unique combustion kinetics and energy release profiles of these sustainable mixtures, a high-fidelity "blend-resolved" parameterization strategy was employed within the digital model. The blending ratios of all fifteen blends utilized in the simulations are detailed in Table 4.

To accurately capture the unique physical and chemical behavior of the alternative fuels, their specific thermochemical properties were explicitly integrated as foundational boundary conditions within the simulation framework. Specifically, the fundamental fluid property sub-models and combustion parameterizations were

**Table 3** Fundamental properties and feedstock origins of the baseline Jet-A and selected SAF alternatives [16]

| Fuel Type | Average Formula | Distillation Profile/°C (IBP/FBP) | Density/15 °C g $cm^{-3}$ | Kinematic Viscosity/-20 °C $mm^2$ $s^{-1}$ | Freezing Point/°C | Flash Point/°C | Net Heat of Combustion/ MJ $kg^{-1}$ | Hydrogen Content/ mass% | Aromatic Content/ mass% |
|---|---|---|---|---|---|---|---|---|---|
| Jet-A | $C_{11.4}H_{21.7}$ | 118 / 295 | 0.8057 | 3.77 | 43.0 | -51.0 | 43.11 | 13.8 | 24.05 |
| FT-SPK | $C_{12}H_{26}$ | 138 / 262 | 0.7597 | 3.44 | 41.5 | < -70.0 | 44.00 | 15.12 | 0.30 |
| HEFA | $C_{15}H_{32}$ | 115 / 298 | 0.7598 | 5.20 | 42.5 | -55.0 | 44.15 | 15.45 | 0.03 |
| ATJ | $C_{12.5}H_{27}$ | 155 / 285 | 0.7596 | 5.23 | 48.5 | < -70.0 | 44.06 | 15.47 | 0.00 |

**Table 4** Volumetric compositions and blending ratios of the investigated SAF and Jet-A mixtures

| Mixture | Jet-A/% | SAF TYPE | SAF/% |
|---|---|---|---|
| ATJ 01 | 90 | ATJ-SPK | 10 |
| ATJ 02 | 80 | ATJ-SPK | 20 |
| ATJ 03 | 70 | ATJ-SPK | 30 |
| ATJ 04 | 60 | ATJ-SPK | 40 |
| ATJ 05 | 50 | ATJ-SPK | 50 |
| FT 01 | 90 | FT-SPK | 10 |
| FT 02 | 80 | FT-SPK | 20 |
| FT 03 | 70 | FT-SPK | 30 |
| FT 04 | 60 | FT-SPK | 40 |
| FT 05 | 50 | FT-SPK | 50 |
| HEFA 01 | 90 | HEFA | 10 |
| HEFA 02 | 80 | HEFA | 20 |
| HEFA 03 | 70 | HEFA | 30 |
| HEFA 04 | 60 | HEFA | 40 |
| HEFA 05 | 50 | HEFA | 50 |

systematically redefined for each evaluated fuel. The critical physicochemical inputs driving these dynamic models—encompassing hydrocarbon composition, physical density, kinematic viscosity, thermal stability limits, and the specific Lower Heating Value (LHV)—are detailed in Table 5. By anchoring the physics-based solver to these exact fuel characteristics, the 1D model dynamically resolves inter-component responses—most notably the instantaneous combustion efficiency, dynamic pressure drop, and total thermal energy release—as a direct thermodynamic consequence of the selected fuel's fundamental chemistry.

## State-dependent emissions

To accurately resolve the emission species within the simulation framework, the fundamental combustion stoichiometry

**Table 5** Blend-resolved thermochemical input parameters for the evaluated fuel configurations [16]

| Mixture | Hydrocarbon Composition/mass% | Density/15 °C g $cm^{-3}$ | Kinematic Viscosity/-20 °C $mm^2$ $s^{-1}$ | Freezing Point/°C | Flash Point/°C | Net Heat of Combustion/ MJ $kg^{-1}$ |
|---|---|---|---|---|---|---|
| ATJ 01 | n-paraffins: 19.0, iso-paraffins: 37.2, cycloparaffins: 22.1, aromatics: 21.7 | 0.8011 | 3.87 | -52.5 | 42.0 | 43.24 |
| ATJ 02 | n-paraffins: 17.0, iso-paraffins: 43.8, cycloparaffins: 19.8, aromatics: 19.5 | 0.7965 | 3.95 | -52.5 | 43.0 | 43.34 |
| ATJ 03 | n-paraffins: 14.9, iso-paraffins: 50.5, cycloparaffins: 17.5, aromatics: 17.1 | 0.7919 | 4.03 | -52.5 | 44.0 | 43.34 |
| ATJ 04 | n-paraffins: 12.9, iso-paraffins: 57.3, cycloparaffins: 15.0, aromatics: 14.7 | 0.7874 | 4.11 | -54.0 | 46.0 | 43.42 |
| ATJ 05 | n-paraffins: 10.8, iso-paraffins: 64.2, cycloparaffins: 12.6, aromatics: 12.4 | 0.7831 | 4.26 | -57.5 | 46.0 | 43.53 |
| FT 01 | n-paraffins: 19.0, iso-paraffins: 36.9, cycloparaffins: 22.3, aromatics: 21.7 | 0.8010 | 3.75 | -54.0 | 42.5 | 43.11 |
| FT 02 | n-paraffins: 17.0, iso-paraffins: 43.2, cycloparaffins: 20.2, aromatics: 19.5 | 0.7966 | 3.73 | -54.0 | 42.5 | 43.19 |
| FT 03 | n-paraffins: 15.0, iso-paraffins: 49.7, cycloparaffins: 18.1, aromatics: 17.2 | 0.7920 | 3.71 | -54.5 | 42.5 | 43.32 |
| FT 04 | n-paraffins: 13.0, iso-paraffins: 56.2, cycloparaffins: 15.9, aromatics: 14.9 | 0.7874 | 3.69 | -55.0 | 41.5 | 43.54 |
| FT 05 | n-paraffins: 11.0, iso-paraffins: 62.8, cycloparaffins: 13.7, aromatics: 12.6 | 0.7828 | 3.67 | -59.0 | 41.5 | 43.57 |
| HEFA 01 | n-paraffins: 19.8, iso-paraffins: 36.2, cycloparaffins: 22.3, aromatics: 21.7 | 0.8012 | 3.88 | -51.0 | 43.5 | 43.16 |
| HEFA 02 | n-paraffins: 18.6, iso-paraffins: 41.9, cycloparaffins: 20.1, aromatics: 19.5 | 0.7966 | 3.98 | -51.5 | 42.5 | 43.27 |
| HEFA 03 | n-paraffins: 17.4, iso-paraffins: 47.6, cycloparaffins: 17.9, aromatics: 17.1 | 0.7922 | 4.14 | -52.0 | 41.5 | 43.35 |
| HEFA 04 | n-paraffins: 16.2, iso-paraffins: 53.4, cycloparaffins: 15.6, aromatics: 14.7 | 0.7874 | 4.21 | -52.0 | 41.0 | 43.35 |
| HEFA 05 | n-paraffins: 14.9, iso-paraffins: 59.3, cycloparaffins: 13.4, aromatics: 12.4 | 0.7828 | 4.37 | -53.0 | 41.0 | 43.55 |

for each evaluated fuel blend was explicitly defined. The generalized stoichiometric combustion reaction with dry air, expressed in Eq. (1), was utilized to establish the theoretical fuel–air mass balances and the baseline species formation for any given hydrocarbon ($C_xH_y$):

$$C_xH_yO_z + \left(x + \frac{y}{4} - \frac{z}{2}\right)(O_2 + 3.76N_2) \rightarrow xCO_2 + \frac{y}{2}H_2O + 3.76\left(x + \frac{y}{4} - \frac{z}{2}\right)N_2 \quad (1)$$

By integrating these stoichiometric balances into the thermodynamic solver, the theoretical foundation for emission modeling is established. To accurately predict state-dependent emissions, a spatially resolved 1D combustor network (Fig. 3) was configured to replace standard homogeneous combustion assumptions. This architecture explicitly partitions the internal air flow into the pre-diffuser, primary dome, and cooling passages based on the physical PT6 geometry. For steady-state baseline calibration, the compressor delivery (Station 3) boundaries were strictly defined: a total pressure ($P_3$) of 273.45 psi, total temperature ($T_3$) of 1318.02°R, and a baseline fuel-to-air ratio (FAR) of 0.02 [15]. By anchoring the simulation to this detailed aerodynamic network, the solver accurately captures localized primary zone temperatures and specific cooling fractions. Consequently, upon introducing blend-resolved SAF properties, the model autonomously computes dynamic shifts in peak flame temperatures and localized equivalence ratios without relying on external empirical corrections.

To quantify emissions resulting from combustion inefficiency (CO, UHC, and soot), a robust mass partitioning approach was developed based on the chemical fate of the unburned fuel fraction. The central logic of this framework relies on the dynamic adjustment of the partitioning coefficients (α, β, γ) as a continuous function of the sustainable aviation fuel (SAF) blending ratio within the mixture.

The distribution of the unburned mass into carbon monoxide, unburned hydrocarbons, and soot for conventional Jet-A was established based on empirical data from established gas turbine literature [18]. These baseline normalized mass partitioning fractions are defined as:

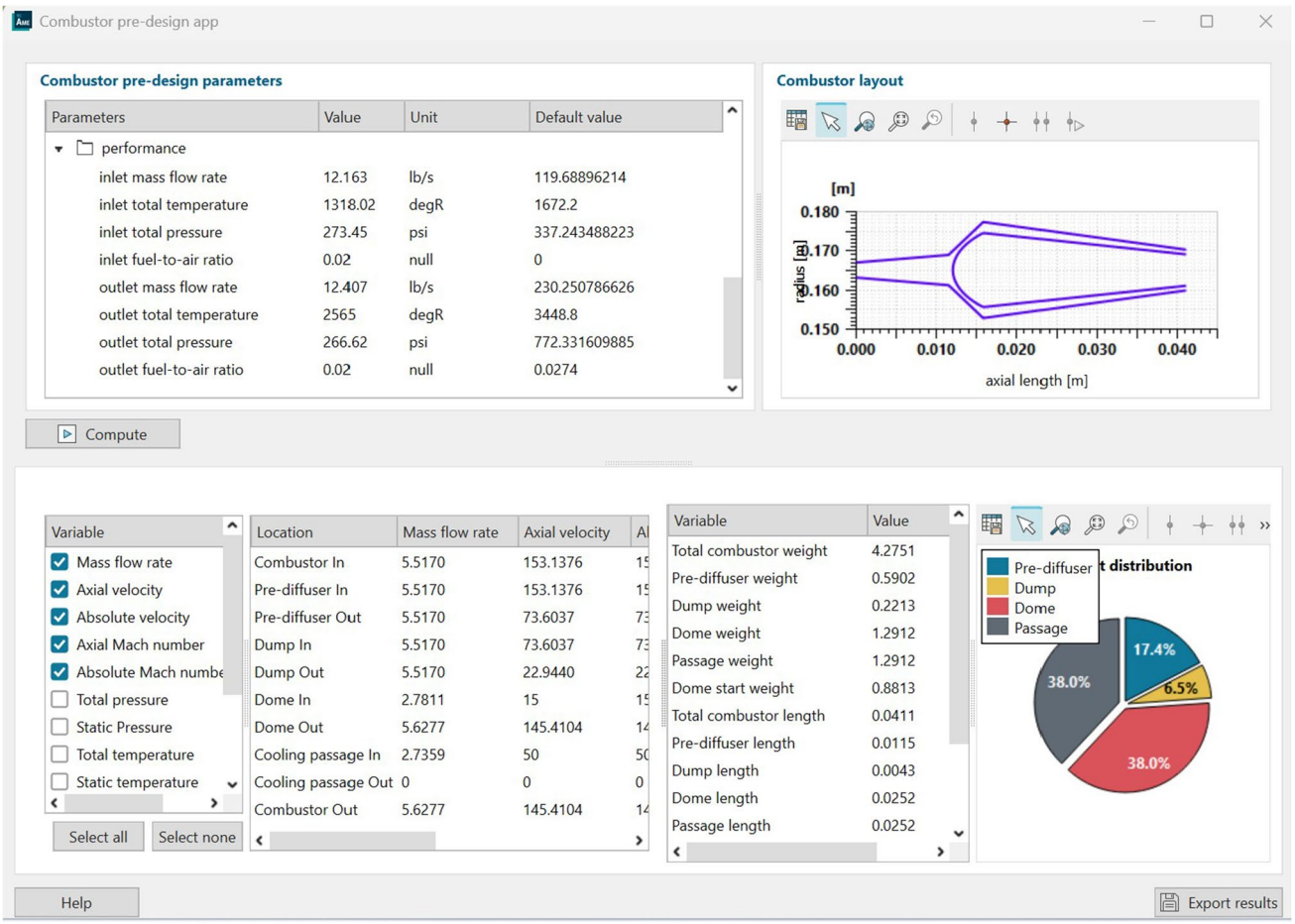


**Fig. 3** Combustor pre-design parameters and air distribution network configured in the software

$$\alpha_{\mathrm{JetA}} = 0.537(CO), \beta_{\mathrm{JetA}} = 0.398(UHC), \gamma_{\mathrm{JetA}} = 0.065(Soot)\# \quad (2)$$

The sum of these coefficients equals unity ($\sum = 1$), ensuring that the entirety of the unburned fuel mass is accounted for across these three pollutant species.

The alternative fuels evaluated (ATJ-SPK, FT-SPK, and HEFA) belong to the synthetic paraffinic kerosene (SPK) family, characterized by zero aromatic content and elevated hydrogen-to-carbon (H/C) ratios. Based on high-pressure combustion test campaigns, neat SPK fuels fundamentally exhibit an approximate 80% reduction in soot formation potential compared to conventional kerosene [19, 20]. Consequently, the baseline soot coefficient ($\gamma_{SAF} = 0.065$) is explicitly reduced by 80% for the pure SAF simulations.

$$\gamma_{\mathrm{SAF}} = 0.013\# \quad (3)$$

To maintain the principle of mass conservation ($\sum = 1$), the residual unburned mass fraction resulting from this soot suppression must be analytically redistributed to the CO and UHC phases. To isolate the primary chemical effects without introducing arbitrary combustion biases, the relative formation ratio between CO and UHC was held constant, strictly consistent with the baseline Jet-A behavior ($\alpha / \beta = 0.537/0.398 \approx 1.349$). By solving this mass conservation constraint, the methodology yields the following physically consistent boundary coefficients for neat SAF:

$$\alpha_{\mathrm{SAF}} = \left(1 - \gamma_{\mathrm{SAF}}\right) x \left[\frac{\alpha_{\mathrm{JetA}}}{\alpha_{\mathrm{JetA}} + \beta_{\mathrm{JetA}}}\right] = 0.0567\# \quad (4)$$

$$\beta_{\mathrm{SAF}} = \left(1 - \gamma_{\mathrm{SAF}}\right) x \left[\frac{\beta_{\mathrm{JetA}}}{\alpha_{\mathrm{JetA}} + \beta_{\mathrm{JetA}}}\right] = 0.420\# \quad (5)$$

This redistribution aligns with experimental observations suggesting that while aromatics suppression drastically reduces particulate matter, the unburned intermediate mass primarily shifts toward gas-phase products rather than disappearing entirely. For any given volumetric SAF fraction ($f_{SAF} \in [0, 1]$), the instantaneous partitioning coefficients are resolved via a linear mixing rule:

$$\alpha_{\mathrm{blend}} = \alpha_{\mathrm{JetA}} . \left(1 - f_{\mathrm{SAF}}\right) + \alpha_{\mathrm{SAF}} . f_{\mathrm{SAF}}\# \quad (6)$$

$$\beta_{\mathrm{blend}} = \beta_{\mathrm{JetA}} . \left(1 - f_{\mathrm{SAF}}\right) + \beta_{\mathrm{SAF}} . f_{\mathrm{SAF}}\# \quad (7)$$

$$\gamma_{\mathrm{blend}} = \gamma_{\mathrm{JetA}} . \left(1 - f_{\mathrm{SAF}}\right) + \gamma_{\mathrm{SAF}} . f_{\mathrm{SAF}}\# \quad (8)$$

The dynamic Emission Indices (EI, expressed in g kg$^{-1}$ fuel) are then extracted by coupling these coefficients with the instantaneous combustion efficiency ($\eta_b$) computed by the physics-based solver:

$$EI_{\mathrm{CO}} = \alpha_{\mathrm{blend}} . \left(1 - \eta_b\right) . 1000\# \quad (9)$$

$$EI_{\mathrm{UHC}} = \beta_{\mathrm{blend}} . \left(1 - \eta_b\right) . 1000\# \quad (10)$$

$$EI_{\mathrm{Soot}} = \gamma_{\mathrm{blend}} . \left(1 - \eta_b\right) . 1000\# \quad (11)$$

It is acknowledged that the linear assumption for soot reduction may exhibit deviations at lower blending ratios due to synergistic chemical effects. Consequently, this methodology is adopted as a first-order engineering approximation, ensuring consistency with simplified emission models such as the FAA AEDT. However, it provides a robust framework for comparative analysis across different SPK types using a unified coefficient set. To maintain methodological consistency across all evaluated pollutants and to capture the full operational advantage of SAF substitution, these mass-based Emission Indices were subsequently translated into power-normalized specific emissions (SE, expressed in g kWh$^{-1}$).

$$SE_i = EI_i . SFC\# \quad (12)$$

Unlike CO, UHC, and soot, which are products of combustion inefficiency, Carbon Dioxide ($CO_2$) is the primary product of complete combustion. Its formation is not dictated by localized quenching or poor atomization, but rather by the fundamental stoichiometric carbon mass fraction (ω_c) of the fuel. Sustainable aviation fuels (SAFs) belonging to the SPK family inherently possess a higher hydrogen-to-carbon (H/C) ratio compared to conventional Jet-A. Consequently, the baseline carbon mass fraction drops from approximately 0.860 in Jet-A to around 0.845 in neat SAF blends [21]. To capture this chemical reduction, the specific carbon mass fraction for any given mixture is dynamically resolved using a linear volumetric blending rule:

$$\omega_{\mathrm{c,blend}} = \omega_{\mathrm{c,JetA}} . \left(1 - f_{\mathrm{SAF}}\right) + \omega_{\mathrm{c,SAF}} . f_{\mathrm{SAF}}\# \quad (13)$$

The standard, state-dependent $CO_2$ Emission Index ($EI_{CO_2}$, in g kg$^{-1}$ fuel) is then calculated by evaluating the stoichiometric conversion of this carbon mass into $CO_2$. This ideal limit is simultaneously penalized by the instantaneous combustion efficiency ($\eta_b$), physically reflecting that unburned fuel mass does not fully oxidize into $CO_2$:

$$EI_{CO_2} = \frac{M_{CO_2}}{M_C} . \omega_{\mathrm{c,blend}} . \eta_b . 1000\# \quad (14)$$

While the classical Emission Index ($EI_{CO_2}$, in g kg$^{-1}$ fuel) only accounts for the fuel's chemical carbon content and combustion efficiency, it does not capture the change in the total fuel mass flow required to produce a given engine

power output. Since SAFs generally have a higher Lower Heating Value (LHV) than Jet-A, the Specific Fuel Consumption (SFC, in kg $kWh^{-1}$) varies with blend ratio. To include this thermodynamic effect into the emission assessment, the power-normalized specific emission ($SE_{CO_2}$, in g $kWh^{-1}$) is introduced. This metric is directly obtained by multiplying the chemical Emission Index by the engine's SFC:

$$SE_{CO_2} = EI_{CO_2}.SFC\# \tag{15}$$

Thermal NOx formation is fundamentally governed by the temperature-dependent Zeldovich mechanism. To analytically capture its nonlinear decay without the computational burden of real-time chemical kinetics, the NOx reduction was modeled using a simplified quadratic surrogate equation:

$$EI_{NOx,blend} = EI_{NOx,JetA}.\left[1 - a.\left(f_{SAF}\right)^2\right]\# \tag{16}$$

where

- $EI_{NOx,JetA}$ is the baseline NOx Emission Index (g $kg^{-1}$ fuel) for neat Jet-A,
- $f_{SAF}$ is the volumetric SAF blend ratio (0 to 1),
- a is a dimensionless coefficient that determines the total reduction when $f_{SAF} = 1$. Consistent with the literature for SPK-class fuels, a has been empirically set to 0.10.

To ensure a fair operational comparison, this mass-based index was subsequently converted into a power-normalized specific emission ($SE_{NOx}$, g $kWh^{-1}$) by integrating the engine's dynamic Specific Fuel Consumption (SFC):

$$SE_{NOx} = EI_{NOx,blend}.SFC\# \tag{17}$$

## Results and discussion

To isolate the fundamental operational impacts of SAF substitution, the turboprop engine was evaluated under a fixed fuel mass flow rate ( $\dot{mfr} = 0.1025$ kg $s^{-1}$) at a constant governed shaft speed of 2000 RPM. This "equal-fuel" boundary condition allows for a direct quantification of how the enhanced energy density of synthetic paraffinic kerosene (SPK) translates into mechanical performance. The comparative results for neat (100%) fuel variants are summarized in Table 6.

Building upon the established theoretical maximums, the operational impacts of practical blending limits (up to 50% volumetric substitution as mandated by ASTM D7566) were analyzed. The linear mixing rules governing the thermophysical properties of the fuel blends resulted in a proportional increase in shaft power. Table 7 details the dynamic response of the engine's mechanical power and Specific Fuel Consumption (SFC) across the intermediate SAF blending ratios (10% to 50%).

The results indicate a definitive thermodynamic advantage for all SAF variants. Driven by the higher gravimetric energy density of the SPK family, the engine autonomously achieved a steady power augmentation. Because the mechanical power output increased while maintaining a constant fuel consumption rate, the SFC exhibited a proportional improvement. This established thermodynamic "premium" dictates that for a given mission power requirement,

**Table 6** Comparative steady-state performance metrics for neat (100%) Jet-A and SAF variants

| Fuel Type | LHV/MJ $kg^{-1}$ | $\dot{mfr}$/kg $s^{-1}$ | Power Output/kW | SFC/kg $kWh^{-1}$ | Δ SFC/% |
|---|---|---|---|---|---|
| Jet-A | 43.20 | 0.10255 | 1071.94 | 0.3444 | Baseline |
| FT-SPK | 44.00 | 0.10255 | 1081.59 | 0.3413 | -0.90% |
| ATJ-SPK | 44.06 | 0.10255 | 1083.02 | 0.3409 | -1.02% |
| HEFA | 44.15 | 0.10255 | 1084.84 | 0.3403 | -1.19% |

**Table 7** Turboprop mechanical power (P) and Specific Fuel Consumption (SFC) for intermediate SAF blends

| Blend Ratio | HEFA Power/kW | HEFA SFC/kg $kWh^{-1}$ | ATJ Power/kW | ATJ SFC/kg $kWh^{-1}$ | FT Power/kW | FT SFC/kg $kWh^{-1}$ |
|---|---|---|---|---|---|---|
| 0% (Jet-A) | 1071.94 | 0.3444 | 1071.94 | 0.3444 | 1071.94 | 0.3444 |
| 10% SAF | 1073.23 | 0.3440 | 1073.05 | 0.3440 | 1072.91 | 0.3441 |
| 20% SAF | 1074.52 | 0.3436 | 1074.16 | 0.3437 | 1073.87 | 0.3438 |
| 30% SAF | 1075.81 | 0.3432 | 1075.26 | 0.3433 | 1074.84 | 0.3435 |
| 40% SAF | 1077.10 | 0.3428 | 1076.37 | 0.3430 | 1075.80 | 0.3432 |
| 50% SAF | 1078.39 | 0.3423 | 1077.48 | 0.3426 | 1076.77 | 0.3429 |

**Table 8** Mass-based chemical Emission Indices (EIi) for intermediate SAF blends

| Blend Ratio | $EI_{CO2}$/g $kg^{-1}$ | $EI_{CO}$/g $kg^{-1}$ | $EI_{UHC}$/g $kg^{-1}$ | $EI_{Soot}$/g $kg^{-1}$ |
|---|---|---|---|---|
| 0% (Jet-A) | 3160.0 | 10.74 | 7.96 | 1.30 |
| 10% SAF | 3148.0 | 10.80 | 8.00 | 1.20 |
| 20% SAF | 3136.0 | 10.86 | 8.04 | 1.10 |
| 30% SAF | 3124.0 | 10.92 | 8.10 | 0.98 |
| 40% SAF | 3112.0 | 10.98 | 8.14 | 0.88 |
| 50% SAF | 3100.0 | 11.04 | 8.18 | 0.78 |

**Table 9** NOx emission reduction via data-driven surrogate modeling

| Blend Ratio/$f_{SAF}$ | $EI_{NOx}$/g $kg^{-1}$ | Reduction in $EI_{NOx}$/% |
|---|---|---|
| 0% (Jet-A) | 8.44 | Baseline |
| 10% SAF | 8.43 | 0.10% |
| 20% SAF | 8.41 | 0.40% |
| 30% SAF | 8.36 | 0.90% |
| 40% SAF | 8.30 | 1.60% |
| 50% SAF | 8.23 | 2.50% |

a SAF-powered engine will inherently consume less total fuel mass.

The emission profile of the combustion process was evaluated using a constant combustion efficiency ($\eta_b = 0.98$), ensuring that the unburned fraction remained uniform across all test points. The mass-based Emission Indices (EI, in g $kg^{-1}$ fuel) for carbon monoxide (CO), unburned hydrocarbons (UHC), soot, and carbon dioxide ($CO_2$) were calculated utilizing the blended chemical partitioning coefficients (α, β, γ).

The absence of aromatic compounds in the SPK-based fuels profoundly altered the combustion byproducts. As demonstrated in Table 8, the most significant environmental benefit was observed in the soot formation; at a 50% blend ratio, the soot Emission Index dropped by exactly 40% (from 1.30 to 0.78 g $kg^{-1}$). The slight proportional increases in CO and UHC are a direct stoichiometric consequence of the shifted hydrogen-to-carbon (H/C) ratio inherent to synthetic paraffins and are consistent with high-pressure combustor literature. Furthermore, the lower carbon mass fraction ($\omega_c$) in SAFs yielded a linear reduction in $CO_2$ mass generation per kilogram of fuel burned.

Thermal NOx formation is fundamentally governed by the temperature-dependent Zeldovich mechanism. To analytically capture its nonlinear decay in response to SAF substitution without the immense computational burden of real-time spatial chemical kinetics, a data-driven impact assessment utilizing a surrogate model was employed. Based on the experimental baseline of the turboprop engine ($EI_{NOx,JetA} = 8.44$ g $kg^{-1}$), the quadratic surrogate equation predicted the emission suppression behavior, as detailed in Table 9.

The surrogate model effectively demonstrates that the reduction in thermal NOx is not strictly linear but accelerates slightly at higher blending ratios. At the maximum permissible 50% blend, the chemical NOx index is reduced to 8.23 g $kg^{-1}$, reflecting the cooler flame temperatures associated with the hydrogen-rich combustion of synthetic paraffins.

To capture the true environmental impact of SAF substitution, the chemical emission reductions ($EI_i$) must be coupled with the engine's improved thermodynamic efficiency. By converting the mass-based indices into power-normalized specific emissions ($SE_i$, in g $kWh^{-1}$) using the engine's dynamic SFC, the "double-benefit" phenomenon becomes explicitly quantifiable, as detailed in Table 10.

The transformation from EI to SE metrics reveals that the actual operational emissions are significantly lower than what chemical analysis alone would suggest. For instance, while the chemical NOx index ($EI_{NOx}$) decreased by 2.50% at a 50% blend, the power-normalized NOx emission ($SE_{NOx}$) decreased by 3.06%. This amplification is the direct result of the turboprop engine operating at a lower SFC. The double-benefit principle validates that integrating data-driven thermodynamic models with chemical partitioning accurately captures the holistic advantages of SAF deployment in aviation gas turbines.

**Table 10** Power-normalized specific emissions (SEi) demonstrating the double-benefit effect

| Blend Ratio | $SE_{CO2}$/g $kWh^{-1}$ | $SE_{Soot}$/g $kWh^{-1}$ | $SE_{NOx}$/g $kWh^{-1}$ | Overall $SE_{NOx}$ Reduction/% |
|---|---|---|---|---|
| 0% (Jet-A) | 1088.30 | 0.447 | 2.906 | Baseline |
| 10% SAF | 1082.91 | 0.412 | 2.899 | 0.24% |
| 20% SAF | 1077.53 | 0.377 | 2.889 | 0.58% |
| 30% SAF | 1072.15 | 0.336 | 2.869 | 1.27% |
| 40% SAF | 1066.79 | 0.301 | 2.845 | 2.09% |
| 50% SAF | 1061.13 | 0.267 | 2.817 | 3.06% |

## Conclusions

This study comprehensively investigated the operational and environmental impacts of substituting conventional Jet-A fuel with synthetic paraffinic kerosene (HEFA, ATJ-SPK, FT-SPK) using a data-driven impact assessment approach based on surrogate models for a turboprop gas turbine engine. By isolating the fundamental combustion and thermodynamic variables, the research quantified the distinct advantages of SAF deployment up to the maximum certified 50% volumetric blend ratio.

The findings reveal a definitive thermodynamic superiority inherent to the SPK family. Operating under a constant fuel mass flow rate constraint, the enhanced gravimetric energy density (LHV) of the SAF variants yielded a direct mechanical power augmentation. Specifically, introducing a 50% HEFA blend resulted in a power increase of approximately 10.5 kW, translating into a 1.0% reduction in Specific Fuel Consumption (SFC). This demonstrates that SAF-powered engines inherently require less total fuel mass to satisfy equivalent mission power demands, with HEFA exhibiting the highest thermodynamic efficiency, closely followed by ATJ and FT-SPK.

Simultaneously, the altered chemical stoichiometry of the synthetic fuels—characterized by the complete absence of aromatics and lower carbon mass fractions—profoundly reshaped the engine's emission profile. While unburned hydrocarbons (UHC) and carbon monoxide (CO) mass indices exhibited marginal, stoichiometrically expected variations (under 3% increase), soot formation demonstrated a dramatic suppression, plummeting by exactly 40% at the 50% blend limit. Furthermore, thermal NOx emissions, evaluated via a data-driven surrogate model to circumvent heavy kinetic computational burdens, exhibited a nonlinear decay, corroborating the cooler flame characteristics associated with hydrogen-rich synthetic paraffins.

The most critical contribution of this research is the mathematical isolation and quantification of the "double-benefit" phenomenon through the power-normalized specific emission ($SE_i$, g $kWh^{-1}$) framework. By integrating the chemical reduction in carbon oxidation with the thermodynamic reduction in total combusted mass driven by the improved SFC, the methodology proves that the actual operational emissions are significantly lower than what isolated chemical mass-balance analyses suggest. At a 50% SAF blend ratio, this synergistic effect yielded net operational emission reductions of 3.1% for $SE_{CO2}$ and 3.06% for $SE_{NOx}$, amplifying the baseline chemical advantages.

Overall, these findings indicate that while synthetic aviation fuels demonstrate excellent drop-in compatibility and immediate, quantifiable environmental benefits, their distinct thermophysical properties slightly shift the optimum operational envelope of legacy engines. Achieving their complete environmental and operational potential necessitates the development of next-generation combustion chamber geometries optimized specifically for SPK-class fuels. In this context, the data-driven impact assessment methodology using surrogate models emerges as an indispensable and highly predictive tool, facilitating the thorough, cost-effective evaluation of advanced fuel-engine integrations within a virtual environment.

**Acknowledgements** This research was supported by TÜBİTAK under project No: 5240035 and by the Centre of Excellence project "Civil Engineering Research Centre" (Grant No S-A-UEI-23–5). This research was supported by the Research Council of Lithuania (LMTLT) under agreement No S-PD-24-180.

**Author Contributions** Doğa Kılıç was involved in data curation; formal analysis; methodology; project administration; visualization; writing—original draft; and writing—review and editing. Melih Yıldız contributed to methodology; validation; writing—original draft; and writing—review and editing. Utku Kale was involved in project administration and resources. Jonas Matijosius contributed to project administration and resources.

**Funding** Open access funding provided by the Scientific and Technological Research Council of Türkiye (TÜBİTAK). No external funding was received specifically for the publication of this research.

**Data Availability** No datasets were generated or analyzed during the current study.

## Declarations

**Competing interests** The authors declare no competing interests.

**Open Access** This article is licensed under a Creative Commons Attribution 4.0 International License, which permits use, sharing, adaptation, distribution and reproduction in any medium or format, as long as you give appropriate credit to the original author(s) and the source, provide a link to the Creative Commons licence, and indicate if changes were made. The images or other third party material in this article are included in the article's Creative Commons licence, unless indicated otherwise in a credit line to the material. If material is not included in the article's Creative Commons licence and your intended use is not permitted by statutory regulation or exceeds the permitted use, you will need to obtain permission directly from the copyright holder. To view a copy of this licence, visit http://creativecommons.org/licenses/by/4.0/.

## References

1. Cabrera E, De Sousa JMM. Use of sustainable fuels in aviation—a review. Energies. 2022;15(7):2440. https://doi.org/10.3390/en15072440.
2. Barke A, Bley T, Thies C, Weckenborg C, Spengler TS. Are sustainable aviation fuels a viable option for decarbonizing air transport in Europe? An environmental and economic sustainability assessment. Appl Sci. 2022;12(2):597. https://doi.org/10.3390/app12020597.
3. Song Z, Li Z, Liu Z. Comparison of emission properties of sustainable aviation fuels and conventional aviation fuels: a review.

Appl Sci. 2024;14(13):5484. https://doi.org/10.3390/app14135484.
4. Klimczyk W, Jasiński R, Niklas J, Siedlecki M, Ziółkowski A. Sustainable aviation fuels: a comprehensive review of production pathways, environmental impacts, lifecycle assessment, and certification frameworks. Energies. 2025;18(14):3705. https://doi.org/10.3390/en18143705.
5. N. Pavlenko, 'Fueling flight: Assessing the sustainability implications of alternative aviation fuels'.
6. D02 Committee, *Specification for Aviation Turbine Fuel Containing Synthesized Hydrocarbons*. https://doi.org/10.1520/D7566-24D.
7. Shahriar MF, Khanal A. The current techno-economic, environmental, policy status and perspectives of sustainable aviation fuel (SAF). Fuel. 2022;325:124905. https://doi.org/10.1016/j.fuel.2022.124905.
8. Marszałek N, Lis T. The future of sustainable aviation fuels. Combustion Engines. 2022. https://doi.org/10.19206/CE-146696.
9. M. Wright, 'Sustainable Aviation Fuel: Technical Certification'.
10. Qasem NAA, et al. A recent review of aviation fuels and sustainable aviation fuels. J Therm Anal Calorim. 2024;149(10):4287–312. https://doi.org/10.1007/s10973-024-13027-5.
11. Yildiz M, Kale U, Nagy A. Analyzing well-to-pump emissions of electric and conventional jet fuel for aircraft propulsion. AEAT. 2022;94(10):1605–13. https://doi.org/10.1108/AEAT-02-2021-0032.
12. 'IATA annual review 2019'. Accessed: May 21, 2025. [Online]. Available: https://www.iata.org/contentassets/c81222d96c9a4e0bb4ff6ced0126f0bb/iata-annual-review-2019.pdf
13. Akbiyik T, Öztürk O, Yıldız M, Kale U, Kilikevičius A. The future of hydrogen fuel in aviation: economic analysis of current applications. Int J Hydrogen Energy. 2025;143:650–8. https://doi.org/10.1016/j.ijhydene.2025.04.324.
14. Dişlitaş AN, Yeşil Ş, Yildiz M. Systems thinking and aircraft design: managing complexity. Aeronaut J. 2026;130(1344):418–33. https://doi.org/10.1017/aer.2025.10090.
15. Zhang Y, Wen M, Wang H. WJ-25 Design Proposal: Proposal for the next generation of Single-Engine Turboprop aircraft. Beijing, China, AIAA Undergraduate Team Design Competition Proposal: Beihang University; 2017.
16. Vozka P, Vrtiška D, Šimáček P, Kilaz G. Impact of alternative fuel blending components on fuel composition and properties in blends with Jet A. Energy Fuels. 2019;33(4):3275–89. https://doi.org/10.1021/acs.energyfuels.9b00105.
17. Kroyan Y, Wojcieszyk M, Kaario O, Larmi M. Modeling the impact of sustainable aviation fuel properties on end-use performance and emissions in aircraft jet engines. Energy. 2022;255:124470. https://doi.org/10.1016/j.energy.2022.124470.
18. Wade MD, Gerstle T. PT6A-68 emissions measurement program summary. Fort Belvoir, VA: Defense Technical Information Center; 2002. https://doi.org/10.21236/ADA412301.
19. Lobo P, et al. Impact of alternative fuels on emissions characteristics of a gas turbine engine – Part 1: gaseous and particulate matter emissions. Environ Sci Technol. 2012;46(19):10805–11. https://doi.org/10.1021/es301898u.
20. Corporan E, et al. Chemical, thermal stability, seal swell, and emissions studies of alternative jet fuels. Energy Fuels. 2011. https://doi.org/10.1021/ef101520v.
21. J. T. Edwards, 'Reference Jet Fuels for Combustion Testing', in *55th AIAA Aerospace Sciences Meeting*, in AIAA SciTech Forum. , American Institute of Aeronautics and Astronautics, 2017. https://doi.org/10.2514/6.2017-0146.

**Publisher's Note** Springer Nature remains neutral with regard to jurisdictional claims in published maps and institutional affiliations.